Terraced spreading of simple liquids on solid surfaces

Ju-xing Yang* and Joel Koplik
Benjamin Levich Institute and Department of Physics, City College of New York, New York, New York 10031

Jayanth R. Banavar
Department of Physics and Materials Research Laboratory, Pennsylvania State University, University Park, Pennsylvania 16802

(Received 6 July 1992)

We have studied the spreading of liquid drops on a solid surface by molecular-dynamics simulations of coexisting three-phase Lennard-Jones systems of liquid, vapor, and solid. We consider both spherically symmetric atoms and diatomic molecules, and a range of interaction strengths. As the attraction between liquid and solid increases we observe a smooth transition in spreading regimes, from partial to complete to terraced wetting. In the terraced case, where distinct monomolecular layers spread with different velocities, the layers are ordered but not solid, with substantial molecular diffusion both within and between layers. The qualitative behavior resembles recent experimental findings, but the detailed dynamics differ. In particular, the layers exhibit an unusual spreading law, where their radii vary in time as $R^2 \sim \log_{10} t$, which disagrees with experiments on polymeric liquids as well as recent calculations.

PACS number(s): 68.10.Gw, 68.45.Gd, 61.20.Ja

I. INTRODUCTION

There are several possibilities for the behavior of a liquid drop placed on a solid surface, depending on the nature of the materials involved and the interactions between them. The traditional classification [1,2] is in terms of nonwetting, partially wetting, and completely wetting cases, and the distinction between them can be nicely conceptualized using Young's equation. Suppose that a liquid (L) drop makes a fixed contact angle θ with a solid (S) surface, with vapor (V) outside the drop. A force balance or the condition of thermodynamic equilibrium yields

$$\gamma_{SV} - \gamma_{SL} - \gamma_{LV} \cos\theta = 0 \ , \tag{1}$$

where γ_{ij} is the free energy per unit area of an interface separating phases i and j. The surface tensions γ_{ij} are measurable or calculable properties of the two phases involved, and the meaning of (1) is that *if* the equation is satisfied with $|\cos\theta| \leq 1$, then θ is the contact angle, and otherwise there is no such equilibrium state. If $\cos\theta < -1$ then it is energetically unfavorable to have liquid and solid in contact, and the drop forms a bead with $\theta = \pi$ or, in the absence of gravity, simply floats away. If instead $\cos\theta > 1$, then it is costly to have the solid exposed to vapor, and the liquid spreads indefinitely to shield the solid. In the latter case of "complete wetting," extensive recent experimental and theoretical work [3–5] has explored the dynamics of spreading, the growth laws for the drop radius and apparent angle, and the behavior of "precursor films" of micrometer thickness which advance ahead of the main drop. Roughly speaking, then, as the liquid-solid attraction increases, one expects stronger coverage of the solid substrate by the liquid and transitions from nonwetting to partial wetting to complete wetting states.

A fascinating very recent development has been the observation of a "terraced wetting" regime for certain nonvolatile polymeric liquids on certain solids with molecularly smooth surfaces [6]. Here, the liquid again spreads completely, but in the form of distinct monomolecular layers of nanometer thickness. The various layers are in the form of disks moving outwards, with radii varying with time as $t^{1/2}$. The bottom layer moves outwards fastest, followed by the second from the bottom, etc., and the upper layers are consumed by the lower ones until eventually only a single monolayer remains. The experimental observations are based on optical interferometric techniques, which have a resolution that is very fine normal to the surface (0.1 Å) but rather coarse parallel to it (200 μm). Little information is known besides the time dependence of the drop shape, and in particular the experiments do not provide any information on the structure of the liquid inside the spreading layers. Likewise, even an empirical classification of those substances exhibiting terraced spreading is not available.

While the existence of terraced wetting is experimentally unambiguous, there is no clear theoretical understanding at present, and in particular it is not known precisely what distinguishes terraced from ordinary complete wetting. Although obviously a collective many-body effect, a continuum description of the spreading process is difficult, since the layers are not thick enough to permit a conventional hydrodynamic description. (A liquid layer thinner than ten or so molecular diameters does not behave as a Newtonian fluid [7].) The only theoretical discussion directly aimed at the phenomenon [8] involves two-dimensional rubberlike sheets which grow by the accretion of molecules at their edges from the layers above and below. The layer profiles satisfy diffusion equations, and in consequence the layer radii

have the $t^{1/2}$ growth seen in the experiments. On the other hand, the absence of diffusion in the interior of the layers must be assumed *ad hoc* and, as we shall see, disagrees with the results presented here. An alternative description is based on a Langevin equation, involving an interfacial profile evolving under the action of attraction to the substrate and thermal fluctuations, and stabilized by surface tension [9]. This model is not specifically aimed at terraced wetting, and does not agree with the experiments, but we mention it because no other theoretical work is available.

In this paper we describe molecular-dynamics (MD) simulations of liquids spreading on solids. The general theme of this work is to construct on a computer an arrangement of atoms and a choice of interactions between them so as to mimic a laboratory experiment on a three-phase system. Although this technique is intrinsically limited to tiny idealized systems observed over miniscule time intervals, it has the advantage of providing detailed microscopic information about the time-dependent atomic configurations. Furthermore, an extensive body of work has shown that MD systems provide a faithful representation of macroscopic phenomena for both equilibrium [10] and nonequilibrium [11] situations, fluid flow problems [12], static drops in isolation [13] and on substrates [14], moving contact lines [15,16], and even interfacial instabilities [17]. As we shall see, all of the wetting regimes can be made to appear in MD simulations by appropriate (and reasonable) choices of parameters, but we focus on the terraced wetting case where additional information is most desirable.

The organization of the paper is as follows. Section II describes the details of the MD simulations used here, and in particular the choice of lattice structures, interaction parameters, and equilibration procedures. We consider two types of liquid—one made of simple spherically symmetric Lennard-Jones (LJ) atoms, while a second involves a more realistic molecular liquid comprised of pairs of LJ atoms nonrigidly tied together with an r^6 attractive interaction. The results of our spreading simulations for one case are discussed in detail in Sec. III, while the changes which occur in variant cases are discussed in Sec. IV. Conclusions, comparison with other approaches, and suggestions for further work appear in Sec. V. Some of our initial results have appeared previously [18].

II. SIMULATION METHOD

To simulate the spreading of a drop, we require a fluid—a liquid plus its vapor—in contact with a solid lattice. The various particles are confined to a rectangular box of size $L\times L\times(H+H_s)$, with periodic boundary conditions imposed on all sides. Initially, the fluid is in the upper region of the box, $0<z<H$, while the lower region $-H_s\le z\le 0$ is a solid wall made of five layers of fcc solid with the (100) surface exposed to the fluid. The solid is thick enough to prevent a direct interaction between the fluid particles on either side. We have worked with several systems: a 4000-atom LJ fluid, with $L=H=60$ and 9000 solid atoms, a 9000 atom LJ fluid with $L=90$ and $H=40$ and 22 500 solid atoms, and a 2000 molecule diatomic fluid, with $L=60$ and $H=30$ and 9000 solid atoms, and finally the same diatomic fluid but a denser substrate with half the lattice spacing.

Turning to the choice of interaction, consider first the atomic fluid systems. The interaction between two atoms of types i and j separated by a distance r is given by a Lennard-Jones potential

$$V_{ij}(r)=\frac{\beta_{ij}}{r^6}\left[\frac{1}{r^6}-\alpha_{ij}\right], \tag{2}$$

where the coefficients are related to the conventional [10] LJ energy and distance parameters ε and σ via $\alpha=\sigma^{-6}$ and $\beta=4\varepsilon\sigma^{12}$, respectively. The fluid subsystem is used as a reference, with all distances expressed in terms of $\sigma\equiv\sigma_{ff}$, masses in terms of the fluid atomic mass m_f, and energies in terms of ε_{ff}. The resulting natural time unit is $\tau\equiv(m_f\sigma_{ff}^2/\varepsilon_{ff})^{1/2}$. The parameter $\alpha\equiv\alpha_{fs}$, the strength of the attraction between fluid and solid molecules, is $O(1)$ and varied in value to produce different wetting regimes. For the solid-solid interactions we choose $\varepsilon_{ss}=50$ and $\sigma_{ss}=2^{-1/6}d$, where $d=\sqrt{2}$ is the lattice constant, so that the equilibrium position of the solid particles is also the minimum of the potential. The mass of the solid particles is $5m_f$. The potentials of fluid-fluid interactions and fluid-solid interactions are cut off at $2.5\sigma_{ff}$ and $2.5\sigma_{fs}$, respectively, and the potential of solid-solid interactions is cut off at $1.8\sigma_{ss}$.

Given the potential, Newton's equations of motion are integrated numerically using the Beeman algorithm [19], with a time step $\Delta t=0.005\tau$. The fluid and solid subsystems are first equilibrated independently for a time interval 20τ, by setting $\alpha=0$ and $\beta_{fs}=1$ and using constant kinetic-energy rescaling. In Fig. 1, the resulting "initial configuration at time $t=0$" for the 4000 fluid-atom system is shown, at temperature $T=0.7$ (in units of ε divided by Boltzmann's constant). At later times, the middle layer of the solid is kept at constant temperature by rescaling of the velocities of the particles in that layer only, in analogy to a laboratory experiment where the solid substrate is kept at a constant temperature. This serves to stabilize the temperature of the entire system, providing a constant-volume quasi-canonical ensemble. After equilibration, for a short period of time a constant gravity force is applied to the fluid particles to bring the drop close to the solid surface. When the drop is brought within the interaction range of the solid surface, the gravity force is removed and the velocity of the center of mass of the drop is reset to zero. The drop then is attracted onto the substrate and begins to spread. (In fact, the attraction between the fluid and solid would attract the drop to the surface even without gravity, and this device merely saves time.)

As is evident in the figure, a LJ liquid is fairly volatile, even at this low temperature barely above the freezing point. Furthermore, since the interactions between vapor particles and the liquid particles are the same, the definition of the boundary of the drop is not very clear. The radius of the drop could be determined systematically through the density profile [13], but this method is

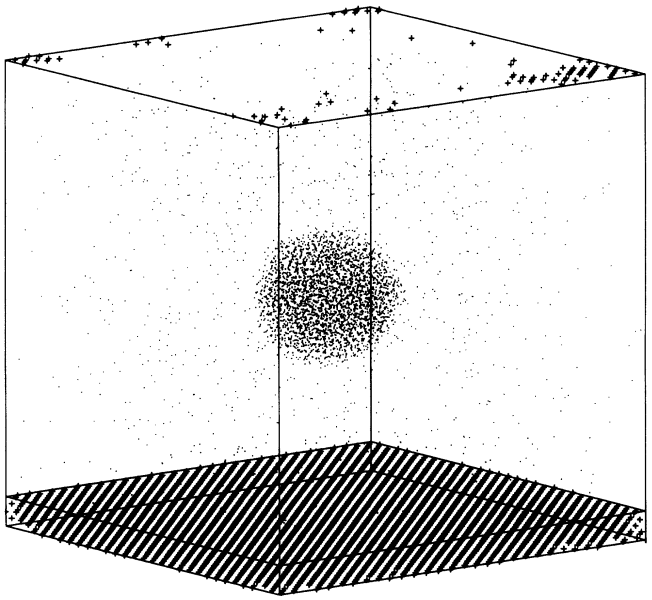

FIG. 1. Initial configuration before spreading-liquid drop plus vapor in a periodic box with a solid substrate. Liquid atoms are shown as dots and solid atoms as plus signs. The solid at the top of the figure represents the periodic image of atoms in the bottom solid layer which have thermally fluctuated below the periodic edge.

problematic after the drop spreads. In this work, we define a drop as a cluster of fluid particles with interparticle distance less than 1.4σ. The radius of the drop determined by both methods is about the same, and equal to 10σ for the 4000 fluid particle system and 13.5σ for the 9000 fluid particle system, respectively.

For the diatomic cases, the liquid atoms are grouped into pairs, and a confining potential

$$V_1(r)=\left[\frac{r}{r_0}\right]^{-12}+\left[\frac{r}{r_0}\right]^{+6}, \tag{3}$$

with $r_0=\sigma/2$, is applied between the two atoms in a pair. This functional form is arbitrary, but serves to maintain the integrity of the molecules. For the reasons discussed in the next section, it is important to consider the spreading of a *nonvolatile* liquid and, as we shall indicate below, this device is sufficient. One might have chosen a harmonic potential instead; we prefer (3) because the r^{-12} core prevents the overlap of the two atoms, and when combined with the rapidly increasing r^6 tail it produces a fairly narrow potential well for which large excursions are unlikely. The minimum of the potential V_1 gives a nominal intramolecular spacing of $r_0\times 2^{1/18}\approx 0.5196\sigma$, and we have found that, for example at temperature $T=1.0$, the actual average spacing of a molecule in a drop is $0.52\pm 0.04\sigma$. In addition to V_1 acting *within* a molecule, the usual LJ potentials described above are applied between each fluid atom and the atoms in all other molecules, and between all fluid and solid atoms.

III. SPREADING DYNAMICS

In this section we discuss in detail the spreading of the 4000-particle atomic fluid system A at a temperature $T=0.7$. These results appear to be generic, and the changes of detail observed in the other cases are discussed in the next section. The key control parameter is the solid-liquid interaction strength α, and independent simulations have been conducted for a range of values $0\le\alpha\le 2.0$. If $\alpha\le 0$, there is no attraction at all between fluid and vapor atoms, and the drop does not wet the solid. For values $0<\alpha\le 1.1$, we observed partial wetting, in which the drop reached a stable spherical cap, while for $\alpha\ge 1.2$ the drop continues to spread up to the boundaries of the simulation box. The transitions between different wetting regimes are apparently smooth.

Typical time sequences for the three classes of spreading process are shown in Figs. 2–4 for $\alpha=1.1$, 1.2, and 1.4, respectively. The points in the figures are the centers of the fluid molecules, where the three-dimensional system has been projected onto the two-dimensional surface of the box. In Fig. 2 a true steady state is reached, with a well-defined contact angle of about 35° (for $\alpha=1.0$ the angle is 50°). In contrast, in Fig. 3 the spreading is slow but does not terminate. Even at $t=800$ the height of the drop is still decreasing while the particle reservoir in the bulk of the drop is nearly depleted. The spreading drop is disordered on the molecular scale, i.e., there is no evident layering, and this case corresponds to "conventional" complete wetting. In Fig. 4, the spreading is complete, and the drop evolves into two distinct molecular layers. Notice that the two layers spread faster than the bulk of the drop, and that the first layer spreads faster than the second. The simulation is terminated when the spreading drop reaches the edge of the periodic box. Note that there *appear* to be fewer molecules as α in-

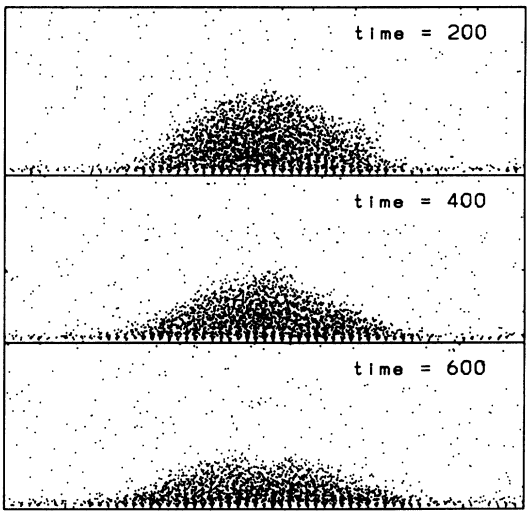

FIG. 2. Snapshots of the 4000-atom LJ-fluid system for $\alpha=1.1$. After time 600 the edge of the drop fluctuates but does not spread further: partial wetting. The points represent the centers of molecules in three dimensions, projected onto the x-z plane. Only molecules with $0<z<20$ are shown.

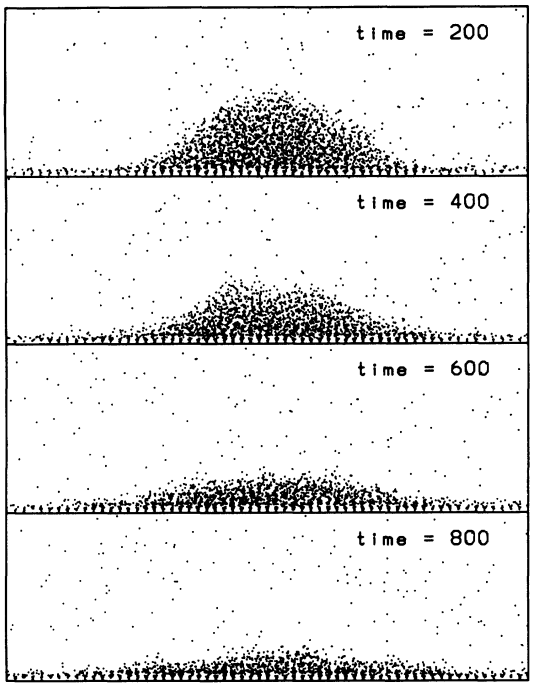

FIG. 3. Snapshots of the 4000-atom LJ-fluid system for $\alpha=1.2$. At later times the liquid in the center continues to spread until uniform coverage is reached: "ordinary" complete wetting.

creases, but this optical illusion is caused by the enhanced ordering in the fluid near the solid surface.

The time variation of the height of the drop, defined as the z coordinate of its center of mass, is shown in Fig. 5 for the $\alpha=1.2$ case. Initially, the drop is driven down by the applied gravity force, and its height decreases quickly. When the drop begins to interact with the substrate, and gravity is removed, the decrease in h slows, and the eventual decay is associated with the transition to uniform coverage. For our subsequent discussion, we require an estimate of the radius of the layers, and this is obtained from the density profile. For example, Fig. 6 shows the density distribution $F(r)$ of the first layer for $\alpha=1.4$ at $t=340$, as a function of in-plane radius r. The "first layer" is defined as those fluid atoms with $0.8<z<1.5$ which are within the drop, according to the definition in the previous section. (The choice of the z limits is motivated by Fig. 8 below.) The particle density in the first layer is roughly a constant, ρ_0, for small r and drops to zero at larger values. We define the radius of the layer R via the relation $F(R)=\rho_0/2$.

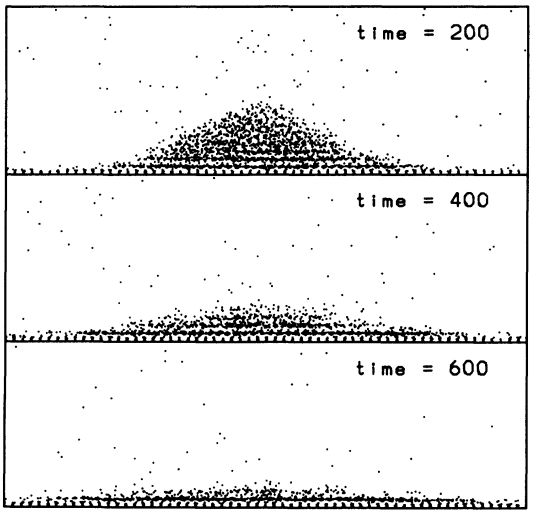

FIG. 4. Snapshots of the 4000-atom LJ-fluid system for $\alpha=1.4$: terraced wetting case.

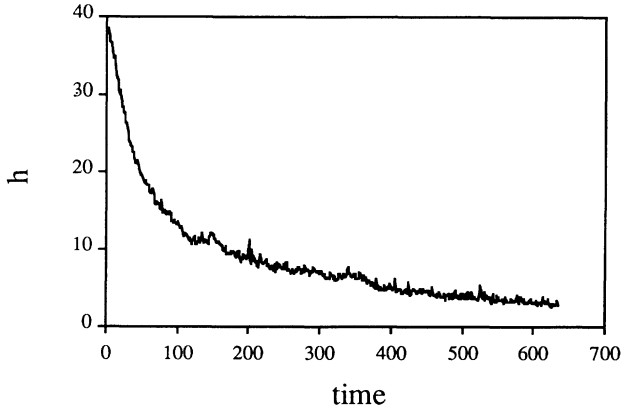

FIG. 5. Height of the drop vs time for $\alpha=1.2$.

In comparing the three cases, we see that the vapor density decreases as α increases due to the condensation of vapor molecules onto the solid wall. Figure 7 displays this condensed layer of regularly spaced molecules for the $\alpha=1.4$ case. In the figure, the lines show the nominal solid lattice and the + signs the instantaneous fluid atomic positions, fully commensurate with the solid structure. The preceding Figs. 2–4 display only those fluid atoms with $z>0$, and therefore omit much of this condensate. The condensation can occur because the lattice spacing is large enough to allow fluid atoms to fill the interstices. The mobility of the particles in the condensed

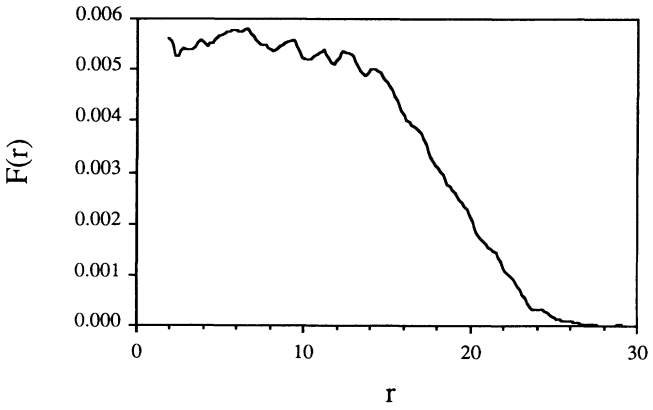

FIG. 6. Density profile of the first layer of a spreading drop for $\alpha=1.4$ at time $t=340\tau$.

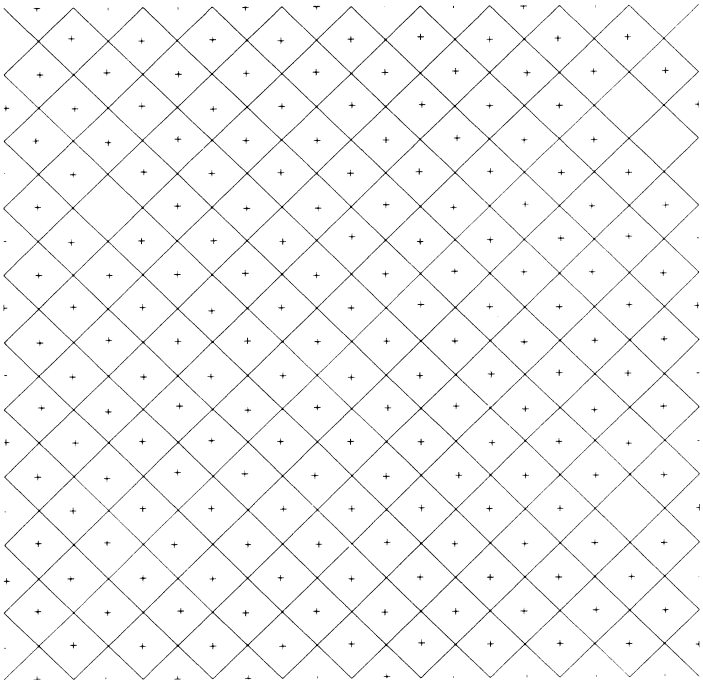

FIG. 7. Molecular positions in the adsorbed fluid layer (+ signs) shown with respect to the lattice axes of the solid substrate (solid grid).

layer is very low, and indeed it forms before the drop spreads to that part of the surface. The existence of the condensed layer should not affect the spreading processes, except insofar as it partially screens the drop from the solid and slightly modifies the solid surface structure.

We proceed to discuss the complete spreading cases in detail. In Fig. 4 one can readily observe the liquid layers near the solid surface. These layers form once the drop is in contact with the solid surface, but layering in liquids near solid surfaces is not in itself novel [20]. The layered structures in drops are shown more clearly by the histogram along the z direction in Fig. 8. In this figure, the first peak indicates the condensed vapor, and the second

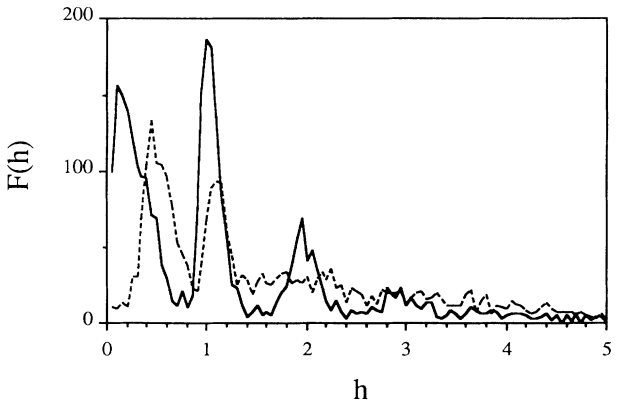

FIG. 8. Density profile in the vertical direction for a spreading drop with $\alpha=1.4$ (solid line) at $t=340\tau$ and $\alpha=1.2$ (dashed line) at time $t=450\tau$.

and third peaks reflect the first and second layers, respectively. In contrast, for $\alpha=1.2$ the location of the first peak (the condensed layer) is higher than that in $\alpha=1.4$ because of the weaker solid-liquid interaction. Also, the third peak (the second layer) in $\alpha=1.2$ is less distinguishable than that in $\alpha=1.4$.

The atomic positions of the first and second layers in terraced spreading are quite strongly ordered. Figures 9(a) and 9(b) show typical x-y projections of the first and second layers for $\alpha=1.4$. The particles form a defective hexagonal lattice, with stronger ordering in the first layer than the second, and within each layer the inner part is more ordered than the outer part. Unlike the condensed layer, Fig. 10 indicates that the nearly ordered first layer is *not* commensurate with the solid surface. This may contribute to the mobility of the particles in the layers, which we discuss further below. The ordering within layers may be further quantified by considering the radial probability distribution functions. Figure 11(a) shows the two-dimensional radial functions for a slab through the center of the liquid drop before contact with the solid. Such a curve is typical of a liquid, with a prominent nearest-neighbor first peak and a rather broad second peak exemplifying short-range ordering. In contrast, Figs. 11(b) and 11(c) show the in-plane two-dimensional radial distribution functions for the first and second layers, respectively. For each layer, we distinguish an inner region $r \le R-5$ (solid curve) and an outer region $R-5<r\le R$ (dashed curve), where R is the radius of the layer as calculated by the procedure described above. We see that the liquid structure in the layers displays considerably more ordering than in the free drop, the peaks be-

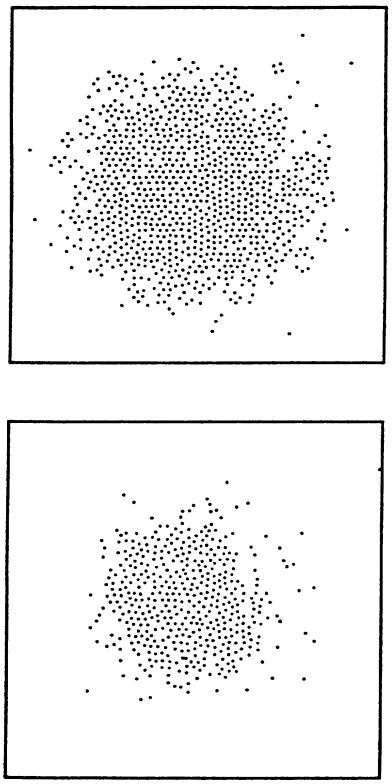

FIG. 9. x-y positions of (a) the first layer and (b) the second layer at $t=340\tau$ for $\alpha=1.4$.

ing higher and narrower, consistent with the visual evidence in Fig. 9.

As the boundaries of the layers move outward, vacancies are created both in the interior and at the edge. By examining the atomic positions as a function of time, one sees that the vacancies in the first layer provide the likely sites for the particles to move in from above. As an illustration, Fig. 12 shows the x-y projection of the first layer at $t=340$ and 341. The dots represent the particles in the first layer at $t=340$, which in this case have stayed in place, and the circles represent particles that were not in the first layer at $t=340$, but moved into the first layer by time 341. The circles are more or less in the defect locations.

Since the fluid layers have a solidlike structure, we may ask if the particles in the layers are really in a liquid, or simply solidified. For this purpose, we calculate the probability distribution function of displacements. Since the spreading is relatively slow, we considered a sliding time window of interval 50τ, averaging over configurations between $t=336$ and 435 for $\alpha=1.4$. We have obtained the vertical probability distribution function $P(\Delta z)$ for displacements normal to the solid surface, as well as the radial probability distribution $P(\Delta r)$ for motion parallel to the surface, separately for the first and second layers of the spreading drop and for various initial radial intervals. To be precise, we define the first layer as $0.8<z<1.5$ and the second as $1.5<z<2.5$, and in each layer we have three regions: I, $0<r<10$; II, $10<r<20$; and III, $20<r<30$, where $r=0$ corresponds to the center of mass of the layer. Note that the vapor which con-

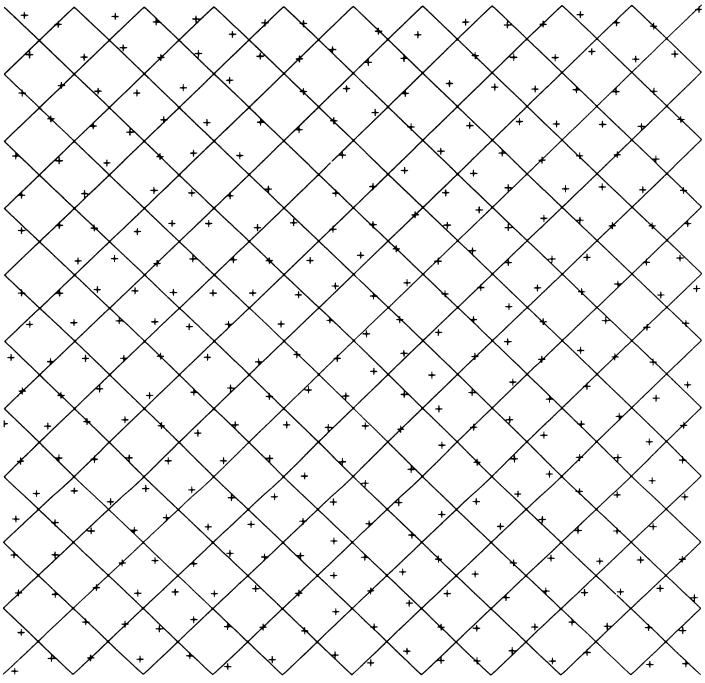

FIG. 10. Molecular positions in the first spreading layer, as in Fig. 7.

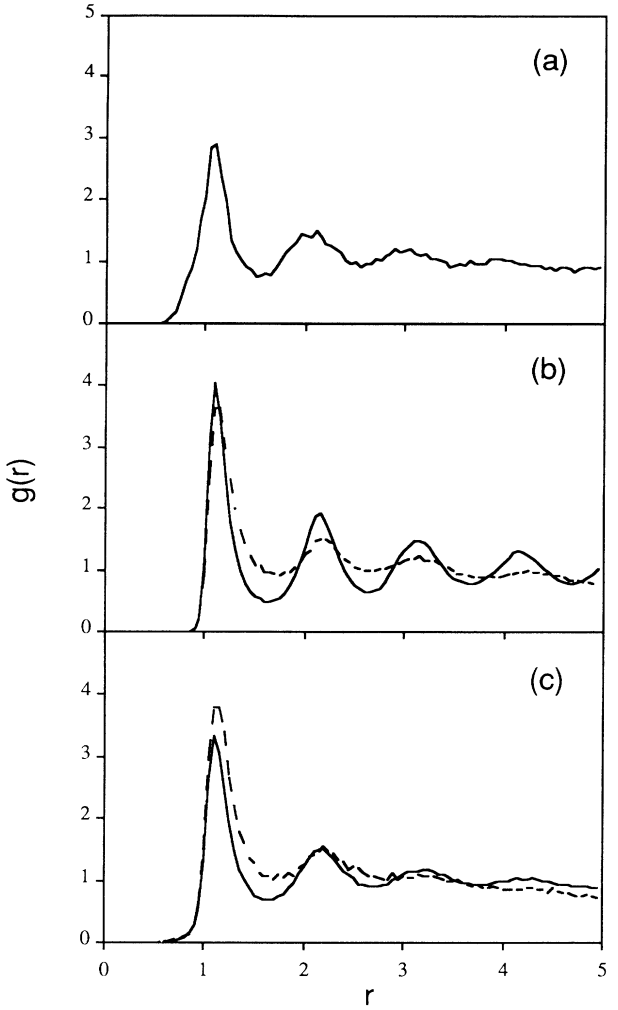

FIG. 11. (a) Two-dimensional radial distribution function for a slab of liquid drop before interacting with the solid. (b) In-plane radial distribution function for the first spreading layer; inner region (solid line) and outer region (dashed line) shown separately. (c) Same as (b) for the *second* spreading layer.

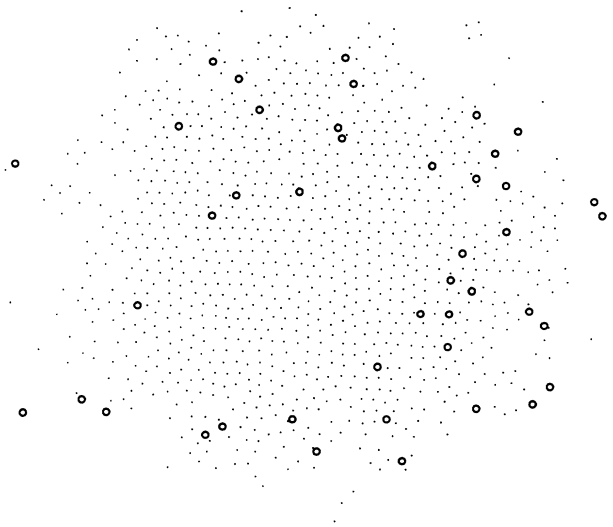

FIG. 12. Atomic positions in the first layer at time 340τ (dots) plus new atoms which migrate into this layer within the next τ (circles).

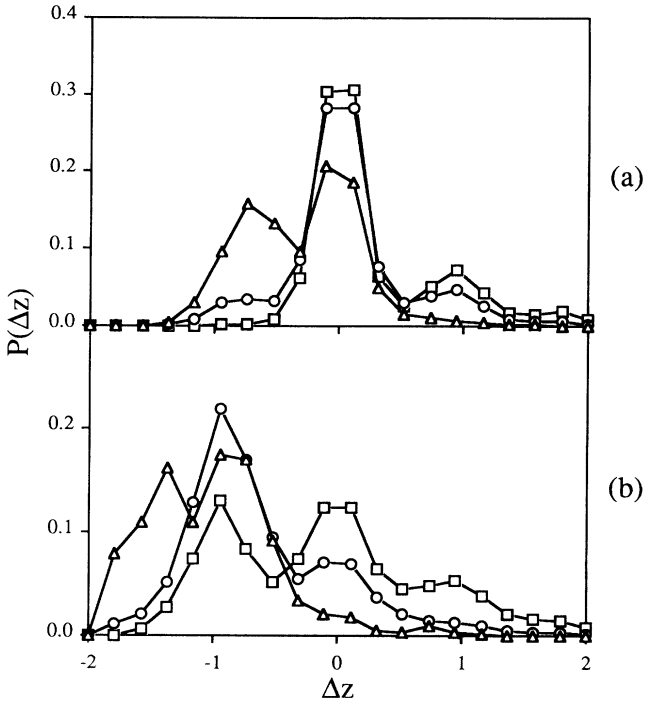

FIG. 13. Vertical probability distribution function $P(\Delta z)$ for (a) the first layer and (b) the second layer. The squares, circles, and triangles represent radial regions I, II, and III, respectively, as specified in the text.

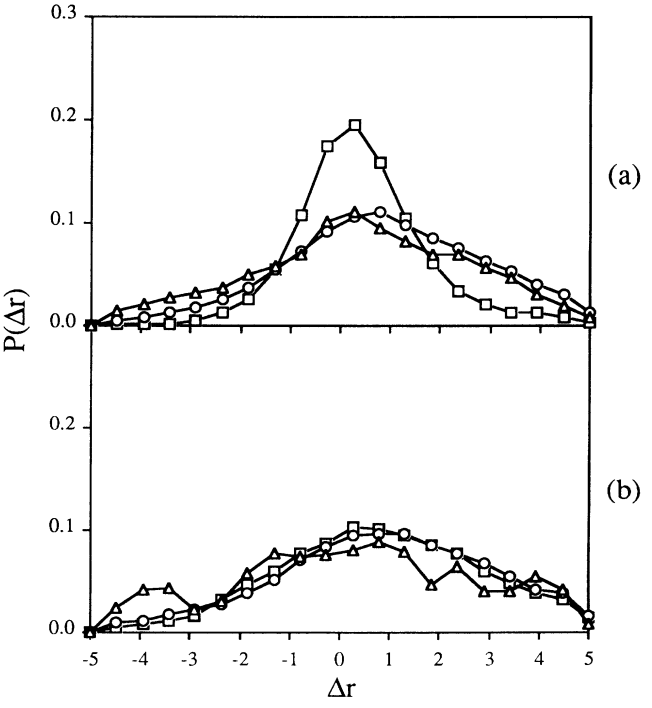

FIG. 14. Radial probability distribution function $P(\Delta r)$, in the same format as Fig. 13.

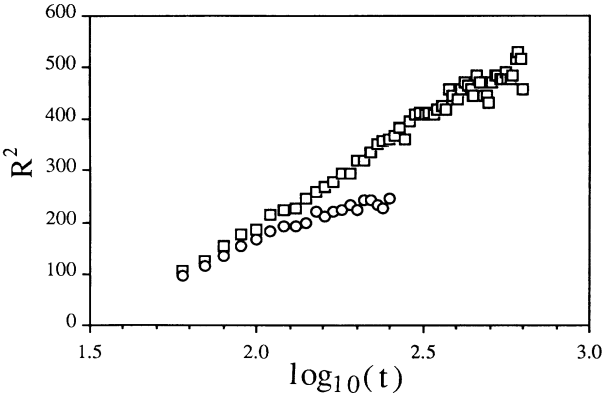

FIG. 15. Dependence of drop radius on time for $\alpha=1.4$ and $T=0.7$ for the first (squares) and second (circles) layers.

densed on the solid surface before the drop spread is rather static and has *not* been included in this analysis.

The distribution of vertical displacements for the first layer is given in Fig. 13(a); we see that for both inner regions I and II the principal peak at $\Delta z=0$ indicates that these molecules tend to stay in the first layer, while the secondary peak at $\Delta z=1$ indicates some probability to jump up to the second layer. In contrast, molecules in outer region III are quite likely to move closer to the solid. In Fig. 13(b) for the second layer, the peak at $\Delta z=-1$ indicates that the principal tendency is to move downwards to the first layer. This tendency decreases as one moves inwards from the outer edge of the layer, so that the inner core is somewhat persistent. Figures 14(a) and 14(b) give the corresponding radial probability distributions for the first and second layers, respectively. The inner ring of the first layer has a peak of unit width favoring small radial displacements, whereas the molecules in region II and III, as well as those in the second layer, have rather broad distributions skewed towards positive Δr. The general conclusion here is that, except for perhaps the inner ring of the first layer, the spreading liquid is not at all rigid or impenetrable. In contrast, the solid substrate itself shows essentially no diffusion between lattice sites over the course of these simulations.

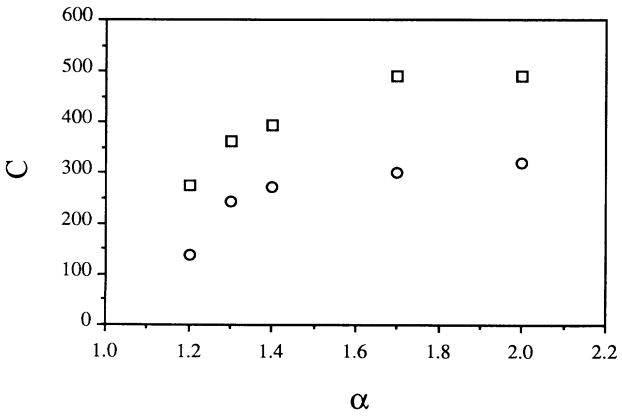

FIG. 16. Coefficient of $\log_{10}t$ in the spreading law (4) for various α: boxes, first layer; circles, second layer.

The next aspect of spreading we consider is the time dependence of the layer radii. Figure 15 shows the evolution of the average radii of the first and second layers as a function of time for $\alpha=1.4$. Evidently, a reasonable fit is

$$R^2(t)=C\log_{10}t+D\ . \tag{4}$$

The first layer's squared radius is consistently of this form, although is a bit ragged towards the end of the simulation where finite sample size effects become more important. The second layer's growth levels off eventually, when the layer runs out of molecules. As usual, a logarithmic variation over a modest time interval is consistent with a weak power law, and a reasonable fit of the form $R^2\sim\sqrt{t}$ is possible. Similar behavior is found for the other values of α where complete wetting occurs. The constant C has been determined for $1.2\leq\alpha\leq2.0$ and the result is shown in Fig. 16. It seems that C increases with α at first, and then saturates.

IV. SPREADING IN MODIFIED SYSTEMS

Although our simulations with LJ atomic liquids show the expected qualitative spreading regimes, the observed $R^2\sim\log_{10}t$ relation disagrees with the (diffusive) $R^2\sim t$ behavior found in laboratory experiments. In order to explore possible explanations for the discrepancy, we have repeated the spreading simulations on several modified systems.

One possible source of difference is the comparatively small number of molecules in the simulation. A laboratory drop has an enormous reservoir of molecules in its center available for continued spreading, whereas here once two distinct layers are visible we have nearly exhausted the supply. Although a 4000-atom fluid is certainly a small system, the results in Fig. 15 are quite consistent with standard finite-size effects, and suggest that a larger drop would continue to spread at the same rate. To verify this statement, we conducted a single run on a larger system, with 9000 fluid molecules and a maximum layer radius of 30. The resulting time series of molecular positions, shown in Fig. 17, are consistent with those of the smaller system. Furthermore, Fig. 18 shows that the growth rate of the layers is well described by the same $R^2=C\log_{10}t+D$ relation, where now $C=571$ and 300 for the first and second layers, respectively. (To be precise, this form applies after an early transient regime where a layer is entirely below the bulk of the drop.) The 9000-atom computation takes us to the limit of our available computer power, requiring about 3 min of CPU time per τ on a Cray-YMP supercomputer. We attempted to extend the calculation to still larger systems by simulating the spreading of a liquid cylinder of radius 19σ in a slab geometry, but in this case the spreading was so slow that the computation proved prohibitive.

Another possible source of concern is the fact that the simulations are conducted at thermodynamic conditions not far from the freezing temperature. We chose a low temperature in the simulations for two reasons: first, to

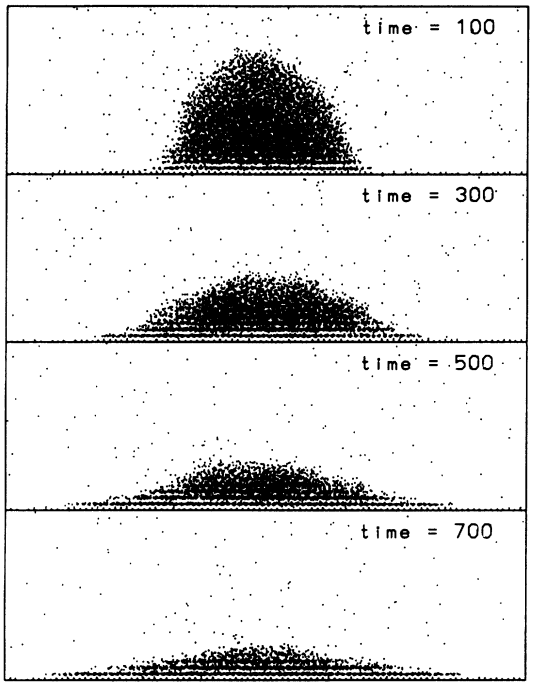

FIG. 17. Time evolution of the spreading of a 9000-atom LJ drop, $\alpha=1.4$.

minimize the amount of vapor in coexistence, and second, to minimize thermal fluctuations in velocity, to attempt to extract a velocity field for comparison with hydrodynamic-based models. (Regrettably, the measured velocity turned out to be indistinguishable from thermal noise.) One might also argue that the formation of the layers is a solidification process which reduces the diffusivity. We performed a simulation with 4000 particles at slightly higher temperature $T=0.8$ with $\alpha=1.4$. The variation of layer radius with time for this case is shown in Fig. 19, and again the $R^2=C\log_{10}t+D$ relation holds. The C values are now 467 for the first layer and

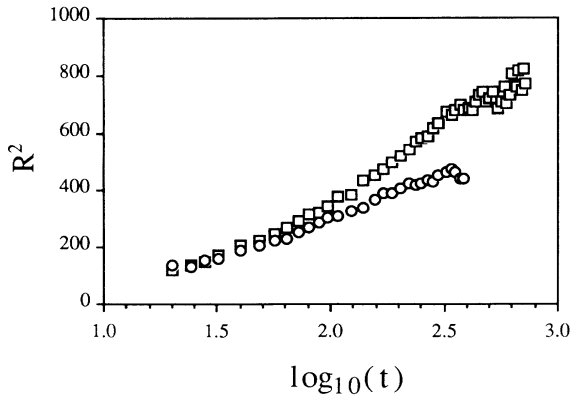

FIG. 18. Growth law corresponding to Fig. 17.

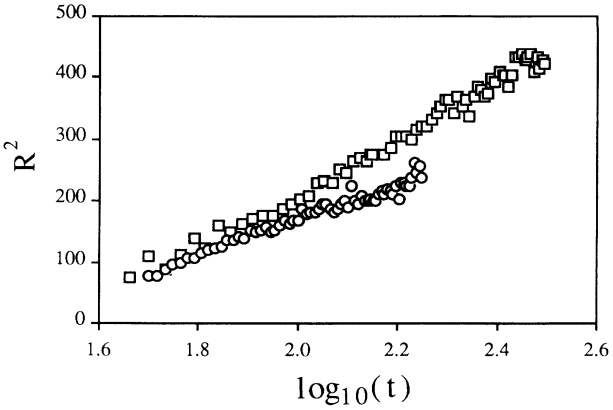

FIG. 19. Growth law for a 4000-atom LJ drop at $T=0.8$.

343 for the second layer. As expected, a higher temperature enhances the mobility of the liquid atoms, and these values are higher than those for $T=0.7$.

Another difference between the present simulations and laboratory experiments is that here the solid-liquid interaction cuts off at a fixed distance (for computational efficiency), whereas a realistic long-range van der Waals potential, arising from a superposition of many layers of r^{-6} interaction, behaves approximately as r^{-3} [20]. In order to check that the partial wetting is not due to this cutoff, we ran a simulation with an extended fluid-solid interaction. This extra potential had the form $k/(z-z_0)^3$ for z (the coordinate normal to the solid surface) greater than the cutoff, with the constants k and z_0 determined by the continuity of the potential. We compared the final states with and without this extended potential for $\alpha=1.0$ and did not see any qualitative changes. In the higher-α cases an additional attraction could only enhance the layering and spreading, so this check was omitted there.

The last remaining obvious difference between the simulations here and the original observations is in the characteristics of the liquid. The experiments [6] were conducted with nonvolatile liquids of appreciable molecular weight (545–2400). It is not feasible at present to perform MD simulations of the dynamics of large ensembles of large molecules, but we *can* deal with the issue of volatility and begin to address the molecular size problem using the dumbbell molecules (DBM's) introduced in Sec. II. Figure 20 shows a time sequence of the terraced spreading of DBM's, where the molecules are shown as lines whose length is the intramolecular spacing. In this case we have chosen $\alpha=3.0$ and temperature $T=1.0$. At lower values of α or T we observe partial wetting; not surprisingly, the parameter values which separate the different regimes are material dependent. Note first the near absence of vapor outside the drop, in comparison with Figs. 2–4. There is an obvious intuitive explanation for the distinction between the two liquids. Roughly speaking, the simple LJ liquid is volatile because if a single spherically symmetric atom is near the edge of the liquid it is easy to thermally fluctuate into the weak tail region of the LJ potential and escape. On the other hand,

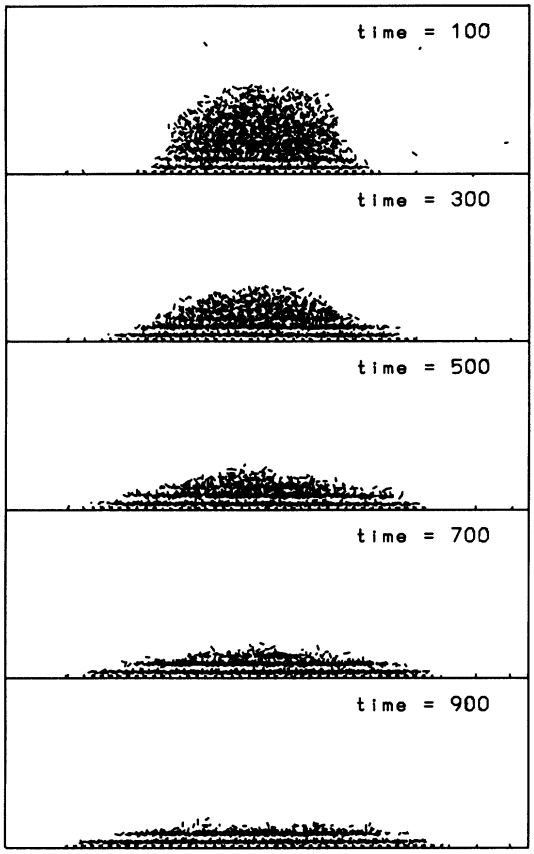

FIG. 20. Snapshots of a DBM drop spreading $\alpha=3.0$ and $T=1.0$. The two atoms in a diatomic molecule are shown as a line segment joining their centers.

in the DBM case an edge molecule vaporizes only if both atoms are in the potential tail, and this configuration is much less likely.

We see that in the DBM system as well, with an appropriate choice of interaction the spreading is in the form of well-defined layers. The growth law of the layers

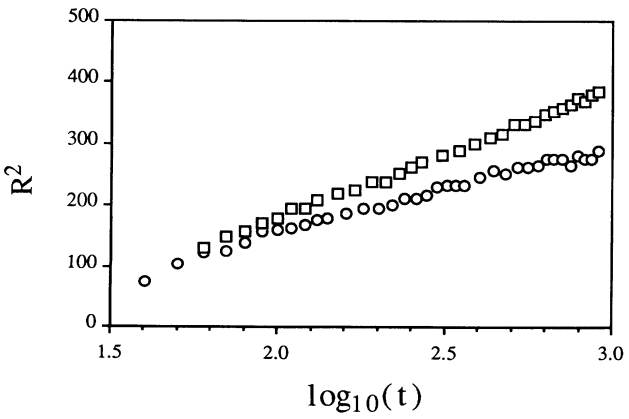

FIG. 21. Growth law corresponding to Fig. 20.

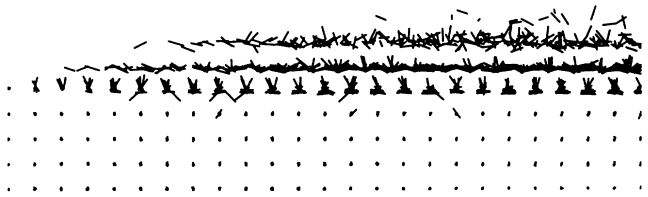

FIG. 22. Orientational order in the spreading of DBM: a snapshot of part of the solid lattice along with adsorbed and spreading layers.

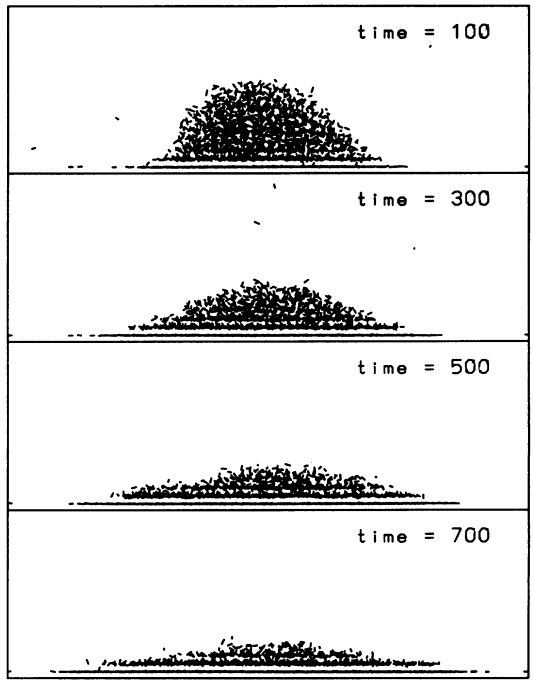

FIG. 23. Snapshots of DBM spreading at $\alpha=3.0$ and $T=1.0$ with the lattice spacing reduced by half.

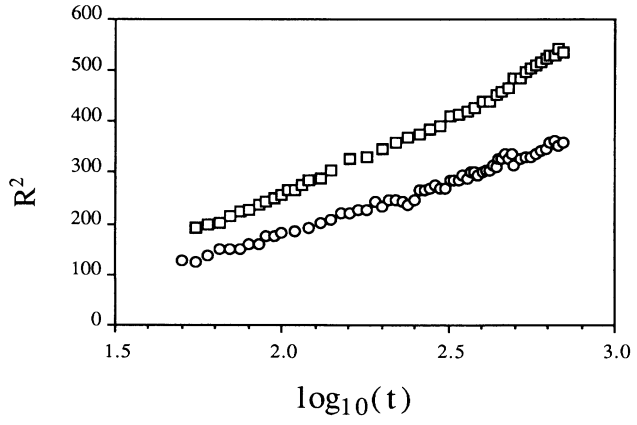

FIG. 24. Growth law corresponding to Fig. 23.

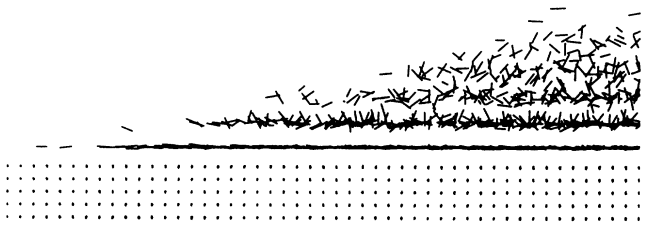

FIG. 25. Close-up view in the reduced lattice spacing case.

is given in Fig. 21, and takes the same $R^2(t) \sim \log t$ form as previously. In this case we find $C=205$ for the first layer, and $C=129$ for the second. One interesting new feature of this system is the spatial orientation of the molecules. In the presence of the strong interaction between liquid and solid atoms, there is an adsorbed layer of liquid, as shown in Fig. 22, where the DBM's prefer to line up vertically. In the first spreading layer, in contrast, the preferred orientation is closer to horizontal, while in the second layer the orientation is more random. To be precise, in the final state, the average orientations relative to the vertical of the condensed, first and second layers are $66\pm27°$, $70\pm18°$, and $62\pm22°$, respectively. The specific molecular configurations are, we believe, determined by the details of the lattice spacing and the choice of interactions, and are therefore rather material dependent. To reconfirm the assertion that the solidification of the spreading liquid is not a factor, we repeated the calculation at $T=1.2$ and found similar results.

One last important check concerns the size of the molecules relative to the lattice spacing. One might question whether the results depend on the fact that the molecules are small enough to fit within the gaps of the lattice and whether the resulting condensate plays a role. To this end, we considered the same DBM fluid spreading on a solid surface with *half* the lattice spacing. The time sequence appears in Fig. 23, the growth law in Fig. 24, and a close-up view of the orientational ordering in Fig. 25. We see that the tightness of the lattice prevents the condensation found in previous cases, and now there is no condensed layer at all. The first spreading layer now finds it energetically advantageous to strongly align parallel to the surface. The average orientations with respect to the vertical are now $85\pm5°$ and $62\pm22°$ for the first and second layers, respectively. Most significantly, the logarithmic growth law still holds for the time dependence of layer radii.

The other extreme in regard to molecule size versus lattice spacing is considered in two recent papers: a MD study of drop spreading with LJ atoms and a smooth, continuum substrate introduced through a z-dependent potential [21], and a Monte Carlo simulation of an Ising-like model for spreading with a similar substrate [22]. These authors find a diffusive spreading law in the appropriate time interval (after initial transients and before the finite volume effects set in, respectively, in the two papers). In our opinion, however, the lack of realism of the solid casts some question on the relevance of the results, since the effects of the corrigations in the potential on the atoms in the spreading molecules are lost, allowing the molecules to slide freely along the solid.

V. CONCLUSIONS

In summary, we have carried out systematic molecular-dynamics studies of the spreading of simple atomic and molecular liquids on a solid surface. We observe that fairly modest variations in the strength of the solid-liquid attraction potential lead to qualitatively different wetting regimes, each with a laboratory counterpart. We have focused on the recently discovered terraced spreading case, where MD is in the best position to provide new information. Although we have clear evidence for spreading in the form of distinct layers, in a variety of systems, the dynamics of the drop size differs in important details from laboratory observation.

The main surprise is in the growth law for the layer radii. The experiments give a diffusive behavior $R^2(t) \sim t$, which is also the obvious theoretical expectation, on the grounds that phenomena at scales below the hydrodynamic continuum are dominated by molecular diffusion. We observe a significantly slower growth, $R^2(t) \sim \log_{10} t$, in a variety of systems. In fact, the variants were selected precisely to address possible explanations of the difference in growth laws. We are left without a convincing explanation, other than the possibility that there are *different* types of spreading, perhaps depending on the details of the interparticle interactions, or molecular structure, or perhaps involving a crossover to a diffusive regime at yet larger scales.

A possible explanation for the discrepancy in growth law originates from the size of the molecules studied here compared with those used experimentally. In the simulation, "small" molecules attempt to diffuse outwards under the pressure of the liquid reservoir, while being restrained by the attraction to the solid substrate. Indeed, the solid lattice provides preferred sites for the fluid atoms, and the growth is associated with hopping between these trapping sites. Many examples of subdiffusive behavior in the presence of traps are known [23], so a slower growth law is not unreasonable. For polymer molecules, however, it is unlikely that many of the atoms in the molecule are in register with the substrate and the trapping might be expected to be less effective. An analogous situation [24] occurs for the flow of liquids in a channel. Polymeric liquids are often non-Newtonian, and have a slip velocity profile, while Newtonian liquids (usually comprised of simpler molecules) exhibit no slip, which corresponds to reduced mobility in the fluid near a solid wall.

Our results for the spreading law also differ from theoretical treatments of the subject. There is at the moment one specific theoretical model relevant to terraced spreading [8], which considers the layer to be rubberlike sheets with diffusive mass transfer at the edges of a layer. We instead observe substantial molecular diffusion everywhere within and on the edges of the spreading drops, so at least for our systems another explanation must be sought. Other theoretical approaches in this general field involve thicker "hydrodynamic" films [4], or generic

solid-on-solid-like models with substrate interactions added [9]. The former approach involves specific assumptions which do not appear to be applicable on the few-molecule scale, while the latter could conceivably be relevant in the sense of being in the correct universality class, but do not in fact seem to have the observed behavior. In general, terraced spreading seems to be a new and only partially understood phenomenon.

ACKNOWLEDGMENTS

This research has been supported by the NASA Microgravity Program and the NSF Fluid, Particulate and Hydraulic Systems Program. Most of the computations were performed using the facilities of the Pittsburgh Supercomputer Center.

*Present address: Department of Biological Chemistry and Molecular Pharmacology, Harvard Medical School, 240 Longwood Ave., Boston, MA 02115.

[1] A. W. Adamson, *The Physical Chemistry of Surfaces,* 4th ed. (Wiley, New York, 1985).
[2] J. S. Rowlinson and B. Widom, *Molecular Theory of Capillarity* (Oxford University, London, 1982).
[3] E. B. Dussan V., Ann. Rev. Fluid Mech. **11**, 371 (1979).
[4] P. G. de Gennes, Rev. Mod. Phys. **57**, 827 (1985).
[5] A. M. Cazabat, Contemp. Phys. **28**, 347 (1987).
[6] F. Heslot, N. Fraysse, and A. M. Cazabat, Nature **338**, 640 (1989); A. M. Cazabat, N. Fraysse, and F. Heslot, Colloids and Surfaces **52**, 1 (1991).
[7] See, e.g., P. A. Thompson and M. O. Robbins, Science **250**, 792 (1991); S. A. Somers and H. T. Davis, J. Chem. Phys. **96**, 5389 (1992).
[8] P. G. de Gennes and A. M. Cazabat, C. R. Acad. Sci. II **310**, 1601 (1990).
[9] D. B. Abraham, P. Collet, J. De Coninck, and F. Dunlop, Phys. Rev. Lett. **65**, 195 (1990).
[10] M. P. Allen and D. J. Tildesley, *Computer Simulation of Liquids* (Oxford University, London, 1987).
[11] W. R. Hoover, Ann. Rev. Phys. Chem. **34**, 103 (1983).
[12] *Microscopic Simulation of Complex Flows,* edited by M. Mareschal, Vol. 236 of NATO ASI Series B: Physics (Plenum, New York, 1990).
[13] S. M. Thompson, K. E. Gubbins, J. P. R. B. Walton, R. A. R. Chantry, and J. S. Rowlinson, J. Chem. Phys. **81**, 530 (1984).
[14] J. Hautman and M. L. Klein, Phys. Rev. Lett. **67**, 1763 (1991), and references cited therein.
[15] J. Koplik, J. R. Banavar, and J. F. Willemsen, Phys. Fluids A **1**, 781 (1989).
[16] P. A. Thompson and M. O. Robbins, Phys. Rev. Lett. **63**, 766 (1989).
[17] J. Koplik and J. R. Banavar (unpublished).
[18] J.-x. Yang, J. Koplik, and J. R. Banavar, Phys. Rev. Lett. **67**, 3539 (1991).
[19] D. Beeman, J. Comput. Phys. **20**, 130 (1976).
[20] J. N. Israelachvili, *Intermolecular and Surface Forces* (Academic, New York, 1985).
[21] J. A. Niemenen, D. B. Abraham, M. Karttienen, and K. Kaski, Phys. Rev. Lett. **69**, 124 (1992).
[22] J. De Coninck, N. Fraysse, A. M. Cazabat, F. Heslot, and P. Levinson (unpublished).
[23] S. Havlin and D. ben-Avraham, Adv. Phys. **36**, 695 (1987); J.-P. Bouchaud and A. George, Phys. Rep. **195**, 127 (1990).
[24] We thank Mark Robbins for suggesting the analogy.